https://doi.org/10.5194/tc-2021-284
Preprint. Discussion started: 21 September 2021

The Cryosphere Discussions
Open Access
EGU

Reassessing seasonal sea ice predictability of the Pacific-Arctic sector using a Markov model

Yunhe Wang[1,4], Xiaojun Yuan[2], Haibo Bi[1,3,4], Mitchell Bushuk[5], Yu Liang[1,6], Cuihua Li[2], Haijun Huang[1,3,4,6]

[1] CAS Key Laboratory of Marine Geology and Environment, Institute of Oceanology, Chinese Academy of Sciences, Qingdao, China.

[2] Lamont-Doherty Earth Observatory of Columbia University, New York, USA.

[3] Laboratory for Marine Geology, Qingdao National Laboratory for Marine Science and Technology, Qingdao, China.

[4] Center for Ocean Mega-Science, Chinese Academy of Sciences, Qingdao, China.

[5] National Oceanic and Atmospheric Administration/Geophysical Fluid Dynamics Laboratory, Princeton, New Jersey, USA

[6] University of Chinese Academy of Sciences, Beijing, China

Corresponding author: Xiaojun Yuan (xyuan@ldeo.columbia.edu)

https://doi.org/10.5194/tc-2021-284
Preprint. Discussion started: 21 September 2021

Abstract

In this study, a regional linear Markov model is developed to assess seasonal sea ice predictability in the Arctic Pacific sector. Unlike an earlier pan-Arctic Markov model that was developed with one set of variables for all seasons, the regional model consists of four seasonal modules with different sets of predictor variables, accommodating seasonally-varying driving processes. A series of sensitivity tests are performed to evaluate the predictive skill in cross-validated experiments and to determine the best model configuration for each season. The prediction skill, as measured by the percentage of grid points with significant correlations (PGS), increased by 75% in the Bering Sea and 16% in the Sea of Okhotsk relative to the pan-Arctic model. The regional Markov model's skill is also superior to the skill of an anomaly persistence forecast. Sea ice concentration (SIC) trends significantly contribute to the model skill. However, the model retains skill for detrended sea ice extent predictions up to 6 month lead times in the Bering Sea and the Sea of Okhotsk. We find that surface radiative fluxes contribute to predictability in the cold season and geopotential height and winds play an indispensable role in the warm-season forecast, contrasting to the thermodynamic processes dominating the pan-Arctic predictability. The regional model can also capture the seasonal reemergence of predictability, which is missing in the pan-Arctic model.

https://doi.org/10.5194/tc-2021-284
Preprint. Discussion started: 21 September 2021

1 Introduction

Sea ice acts as a major component of the Arctic climate system through modulating the radiative flux, heat, and momentum exchanges between the ocean and the atmosphere (Peterson et al., 2017; Porter et al., 2011; Smith et al., 2017). Sea ice also modulates sea surface salinity, which is one of the key drivers for thermohaline circulations (Sévellec et al., 2017). The rapid retreat of Arctic sea-ice extent in the past few decades has been considered a key indicator of climate change (Koenigk et al., 2016; Notz and Marotzke, 2012; Swart, 2017). The shrinking Arctic sea ice contributes to polar temperature amplification (Kim et al., 2016; Screen and Francis, 2016), an increase in wintertime snowfall over Siberia, northern Canada, and Alaska (Deser et al., 2010), polar stratospheric cooling (Screen et al., 2013; Wu et al., 2016), and potentially contributes to a weakening of the mid-latitude jet (Francis and Vavrus, 2012) and increased frequency of cold Northern Hemisphere midlatitude winter events (Cohen et al., 2020; Meleshko et al., 2018).

Also, the rapid summer Arctic sea ice retreat has created more commercial opportunities in the newly opened Arctic waters. The Northwest Passage (through northern Canada) and the Northern Sea Route (north of Russia) could offer faster and less expensive shipping between the Pacific and Atlantic (Smith and Stephenson, 2013). Information on the Arctic marine accessibility and ice-free season duration in the marginal ice zone would enable planning of merchant shipping, conservation efforts, resource extraction, and fishing activities. The growing polar ecotourism industry could also benefit from shrinking sea-ice cover. Therefore, increased efforts have been devoted to developing Arctic sea-ice forecast systems in recent decades.

Substantial efforts have gone toward developing both statistical and dynamical sea ice prediction models. Numerous studies using fully coupled general circulation models (GCMs) have quantified the seasonal prediction skill of pan-Arctic sea ice extent (SIE), which have found forecast skill for detrended pan-Arctic SIE at lead times of 1 to 6 months (Blanchard-Wrigglesworth et al., 2015; Day et al., 2014; Guemas et al., 2016; Peterson et al., 2015; Sigmond et al., 2013). Bushuk et al. (2017)

evaluated regional Arctic sea ice prediction skill in a Geophysical Fluid Dynamics Laboratory (GFDL) seasonal prediction system. They found skillful detrended reigonal SIE predictions, and found that skill varied strongly with both region and season. On the other hand, statistical methods are also appealing for seasonal sea ice predictions (Petty et al., 2017). In some cases, statistical models provide better performance than dynamical models (Hamilton and Stroeve, 2016). For example, Yuan et al. (2016) showed that a linear Markov model has skillful sea ice concentration (SIC) predictions up to 9-month lead times in many regions of the Arctic and that this statistical model consistently captured more sea ice prediction skill than NOAA/NCEP Climate Forecast System (CFSv2) and the Canadian seasonal and interannual prediction system at the seasonal time scale. The Markov model prediction skill also exhibits strong regional and seasonal dependence.

Two common characteristics of sea ice predictability emerged from both dynamic (e.g. CFSv2 and GFDL climate models) and statistical models (e.g. linear Markov models, and linear regression models). First, low prediction skill occurs in the Pacific sector of the Arctic, particularly in the Bering Sea and the Sea of Okhotsk, compared with other Arctic regions (Bushuk et al., 2017; Yuan et al., 2016). Many factors may lead to this low predictability. Bushuk et al. (2017) suggest that less persistent sea ice anomalies in the North Pacific sector possibly lead to less predictability in the region by the GFDL dynamical model. The Markov model of Yuan et al. (2016) was built in multivariate empirical orthogonal functions (MEOF) space in the pan-Arctic and the leading modes are dominated by the large long-term trend and strong climate variability in the Atlantic sector (Figure 1). So the signal of sea ice variability in the Pacific sector could be under-represented in the model. Therefore, it is necessary to evaluate the sea ice predictability in the Pacific sector with a new regional model.

Second, low predictability occurs in the spring months or is initialized in spring (Bushuk et al., 2017; Day et al., 2014; Yuan et al., 2016). Spring sea ice variability is complicated by surface melt ponds. The sea ice driven processes in spring could be different from those in other seasons. In the Pacific sector of the Arctic, sea ice does

https://doi.org/10.5194/tc-2021-284
Preprint. Discussion started: 21 September 2021

not exist during the summer months in the Bering Sea and the Sea of Okhotsk, and sea ice nearly 100% covers the regions within the Arctic Basin in winter. Both cases lead to no sea ice variability and therefore no predictability. Moreover, the Bering Sea opens to the North Pacific, facing a more divergent environment, while sea ice movement is more constrained by the geographic setting of the Arctic Basin in the Chukchi Sea, East Siberian Sea, and the Beaufort Sea. Strong seasonality and geographic setting dictate that different driving processes may play dominant roles in different seasons.

In this study, we develop a regional linear Markov model for the seasonal prediction of SIC in the Pacific sector with a focus on understanding unique sea ice driving processes in different seasons. We follow the framework of the pan-Arctic linear Markov model (Yuan et al., 2016). Unlike the pan-Arctic model that was developed with one set of variables (SIC, surface air temperature, and sea surface temperature) for all seasons and the entire Arctic region, the regional model consists of four modules with seasonal dependent variables, which isolate the dominant processes for each targeted season. Regional relevant predictors are evaluated. New variables, including surface net radiative flux, turbulent heat flux, and pressure and wind fields are introduced to the model experiments. Sea ice predictability is assessed at grid points and over all seasons, and subsequently compared with the pan-Arctic model and other dynamic models.

2 Data and methodology

2.1 Data

We choose to define the atmosphere-ice-ocean coupled Arctic climate system with 7 variables: SIC, sea surface temperature (SST), surface air temperature (SAT), surface net radiative flux, surface net turbulent heat flux, 850 hPa geopotential height, and 850 hPa wind vector. Monthly SICs in 25km × 25km grids are obtained from the National Snow and Ice Data Center (NSIDC) from 1979 to 2020 (Comiso, 2017). The dataset is generated from brightness temperatures derived from Nimbus-7 Scanning

Multichannel Microwave Radiometer (SMMR), Defense Meteorological Satellite Program (DMSP) –F8, -F11, and -F13 Special Sensor Microwave/Imager (SSM/I), and DMSP-F17 Special Sensor Microwave Imager/Sounder (SSMIS) using the bootstrap algorithm. All atmospheric and oceanic variables with a spatial resolution of 1° × 1° are from the latest European Centre for Medium-Range Weather Forecasts (ECMWF) reanalysis product ERA5 (Hersbach et al., 2020) and are applied to represent the conditions of the atmosphere and ocean. ERA5 is produced using the version of ECMWF's Integrated Forecast System (IFS), CY41R2, based on a hybrid incremental 4D-Var system, with 137 hybrid sigma/pressure (model) levels in the vertical direction, with the top-level at 0.01 hPa.

2.2 The model

The idea of using a Markov model for climate prediction is to build multivariate models, aiming to capture the co-variability in the atmosphere-ocean-sea ice coupled system instead of linearly regressing on individual predictors. Yuan et al. (2016) applied this statistical approach to predict SIC in the Arctic at a seasonal timescale and showed that the Lamont statistical model outperformed the NOAA CFSv2 operational model and the Canadian Seasonal to Interannual Prediction System in sea ice prediction. They used multivariate empirical orthogonal functions (MEOF) as the building blocks of the model to filter out incoherent small-scale features that are basically unpredictable. Similar Markov models were also developed to study ENSO predictability (Cañizares et al., 2001; Xue et al., 2000) and for East Asian monsoon forecasts (Wu et al., 2013). The success of the Markov model is attributed to the dominance of several distinct modes in the coupled atmosphere-ocean-sea ice system and to the model's ability to pick up these modes.

Here we focus on the atmosphere-ocean-sea ice interactive processes that are unique to the Pacific sector and develop a regional linear Markov model for the seasonal prediction of SIC. The model consists of four modules with seasonally dependent variables. The model area extends from 40°N to 84°N in latitude and from 120°E to 240°E in longitude. For the sea ice field, the grid cells where the number of

https://doi.org/10.5194/tc-2021-284
Preprint. Discussion started: 21 September 2021

months with variable SIC (15%-95%) is less than 4% of the total time series (492 months) are masked and excluded together with land grid cells. Our model is constructed in the MEOF space. The base functions of the model's spatial dependence consist of the eigenvectors from the MEOF, while the temporal evolution of the model is a Markov process with its transition functions determined from the corresponding principal components (PCs). We use only several leading MEOF modes, which greatly reduce model space and filter out unpredictable small-scale features. This method of reducing model dimension has been successfully used in earlier Antarctic and Arctic sea ice predictability studies (Chen and Yuan, 2004; Yuan et al., 2016).

We preselect SIC, SST, SAT, surface net radiative flux, surface net turbulent heat flux, and geopotential height and winds at 850 hPa to represent different sea ice-driving processes in the Pacific sector. The initial multivariate space is formed to capture the predictable variability in the atmosphere-ice-ocean system by MEOF analysis. Since our focus is on short-term climate variability, the climatological seasonal cycle for the period from 1979 to 2020 was subtracted to obtain monthly anomalies for all variables. A normalization is applied to the time series at each grid point for all variables. To emphasize sea ice variability in the model construction, we weight SIC by 2 and other variables by 1, although the final model skill is not very sensitive to this choice of weight. The weighted variables are stacked up into a single matrix $\mathbf{V}$(n, m), where n is the number of grid points of all fields and m is the length of the time series. We then decompose $\mathbf{V}$ into eigenvectors (spatial patterns) $\mathbf{E}$ and their corresponding PCs (time series) $\mathbf{P}$:

$$\mathbf{V} = \mathbf{E}\mathbf{P}^{T}, \quad (1)$$

where the columns of $\mathbf{E}$ are orthogonal and the columns of $\mathbf{P}$ are orthonormal; the superscript T denotes matrix transpose. It greatly reduces the model space by truncating (1) to the several leading modes. The Markov model is computed using the single-step correlation matrix, that is, a transition matrix $\mathbf{A}$ that satisfies the following linear relation:

https://doi.org/10.5194/tc-2021-284
Preprint. Discussion started: 21 September 2021

$$P_{i+1} = AP_i + e_i, \quad (2)$$

where i denotes the ith month and e_i is the error in the model fit. Transition **A** is calculated by multiplying (2) with P_i^T

$$P_{i+1}P_i^T = AP_iP_i^T + e_iP_i^T, \quad (3)$$

For the best model fit, e_i and P_i^T should have no correlation. Thus

$$A = (P_{i+1}P_i^T)(P_iP_i^T)^{-1}. \quad (4)$$

A is constructed to be seasonally-dependent because of the strong seasonality of SIC and related variables. Thus (4) is applied to 12 subsets of PCs to obtain different transition matrices for each of the 12 calendar months.

After the Markov model is formulated, the SIC prediction can be made through the following eight steps: 1) to examine which variables have highest prediction potential in the Pacific sector, we create 10 climate variable combinations representing different driving processes. 2) The PCs corresponding to each initial multivariate space are calculated by the MEOF equation (1). 3) Transition matrices, **A**, for each calendar month are calculated by equation (4). 4) The predictions of the PCs are made by truncating to the first several modes and applying the appropriate transition matrices at different lead times. "Lead time" refers to the number of months prior to the target month that the forecast was initialized. For example, lead-1 prediction of January SIE is based on December data. 5) The predicted PCs are combined with the respective eigenvectors to produce a spatially-resolved SIC anomaly prediction for each variable combination. 6) We evaluate the prediction skill measured by the SIC anomaly correlation coefficient (ACC), percentage of grid points with significant ACC (PGS), and root mean square error (RMSE) using cross-validated model experiments to identify the superior model for each season. 7) The complete SIC anomaly prediction can then be generated by combining predicted PCs by the corresponding optimal model in each season with eigenvectors. We differentiate the seasons as follows: winter (December through February), spring (March through May), summer (June through August), and autumn (September

https://doi.org/10.5194/tc-2021-284
Preprint. Discussion started: 21 September 2021

through November). 8) The predicted SIC anomalies are divided by weight value 2, multiplied by standard deviation, and added the climatology to generate the complete prediction field.

To determine model variables and the number of modes to be used in the model, we evaluate the prediction skill at all grid points and all seasons in a cross-validated fashion for the period 1980-2020, by calculating the ACC and RMSE between predictions and observations. Notably, the dramatic declining trend in SIC prohibits us to use the first half of the time series for training the model and the second half of the time series to validate the model since the climate system mean state has changed dramatically over the last four decades. Another cross-validation scheme (Barnston and Ropelewski, 1992) is jackknifing, where one case is withheld from the regression development in the Markov model as an independent sample for testing. Thus, we built a Markov model for each month with a 1-yr moving window of data removal, and then used this window of data to evaluate model predictions. Here, we subtract one-year data from PCs and recalculate the transition matrix in equation (4); then twelve-month predictions are generated for that year. This procedure is repeated for each year of the time series. Such a cross-validated experimental design reduces artificial skill without compromising the length of the time series.

The long-term trend is an essential part of the Arctic sea ice variability. A substantial declining trend exists in Arctic SIC, particularly in the Barents Sea, the Kara Sea, the Beaufort Sea, and the Chukchi Sea (Figure 1). However, outside of the Arctic Basin, the long-term trends are relatively weak in the Pacific sector. As the trends are parts of the total variability, we retain the SIC trends in anomalies while building the model and then conduct a post prediction evaluation of the impact of trends on the model skill.

https://doi.org/10.5194/tc-2021-284
Preprint. Discussion started: 21 September 2021

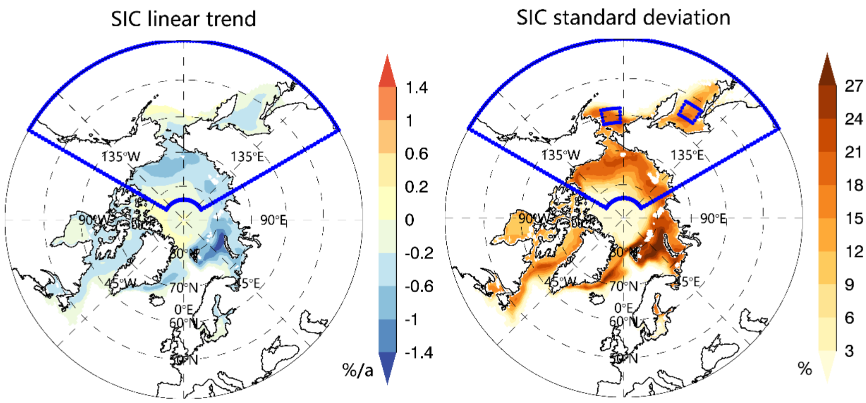

Figure 1. Arctic SIC trends (left) and standard deviation (right) computed using SIC anomalies over all 12 months of the period 1979-2020. The Pacific-Arctic model domain is enclosed by blue lines, which covers 40° - 84°N and 120° - 240°E. Two focused areas marked in blue boxes in the Bering Sea (between 58°- 62°N and 182°-192°E) and the Sea of Okhotsk (between 52°- 56°N and 144°-152°E) have large standard deviations and are selected to evaluate the ACC skill improvement in the regional model compared with the pan-Arctic Markov model developed by Yuan et al. (2016).

3 Model construction and assessments

3.1 EOF analysis of Pacific SIC

Before constructing the model, we first examine whether the EOF analysis can isolate the regional and seasonal SIC variability in the Pacific−Arctic sector. Figure 2 shows the eigenvectors of the three leading EOF modes of SIC. The first mode of SIC variability, accounting for 23% of the total variance, mainly shows a positive pattern within the Arctic Basin from 1979 to 2002 and a negative pattern after 2003 with a record low in 2007 and 2012, representing the decreasing trend in summer and early fall SIC. The declining trend is heavily loaded inside the Arctic Basin from the East Siberian Sea to the Beaufort Sea. The second SIC mode (9% of total variance) primarily captures out-of-phase SIC anomalies in the Bering Sea and the Sea of Okhotsk with a positive pattern in the Bering Sea after 2004 and an opposite phase in

https://doi.org/10.5194/tc-2021-284
Preprint. Discussion started: 21 September 2021

the Sea of Okhotsk, which represents SIC variability in cold seasons and is associated with the Aleutian-Icelandic low seesaw (Frankignoul et al., 2014). The SIC variability in the central sector (approximately 60°-70°N) stands out in the third EOF mode (7% of the total variance), which is a commonly observed feature in the region during spring and autumn. This finding shows that the EOF (MEOF) analysis can well isolate the regional and seasonal SIC variability including the trend in the Pacific-Arctic sector. We further divided the SIC time series into four seasons and conducted EOF analysis respectively. The results show that fewer modes can explain the dominant SIC variance in autumn and summer benefiting from the large SIC variability and trend (Figure S1). For example, the leading 10 modes can explain 70% of the SIC total variance in autumn and summer, while about 25 modes are needed for the cold season. It turns out that the several leading modes can explain the dominant SIC variability. This is an important premise to reduce the model dimension and, more importantly, to filter out incoherent small-scale features that are likely unpredictable. In addition, it is necessary to build the sea ice prediction model for individual seasons because of the differences in seasonal patterns of variability and the different number of leading modes required to capture this variability.

https://doi.org/10.5194/tc-2021-284
Preprint. Discussion started: 21 September 2021

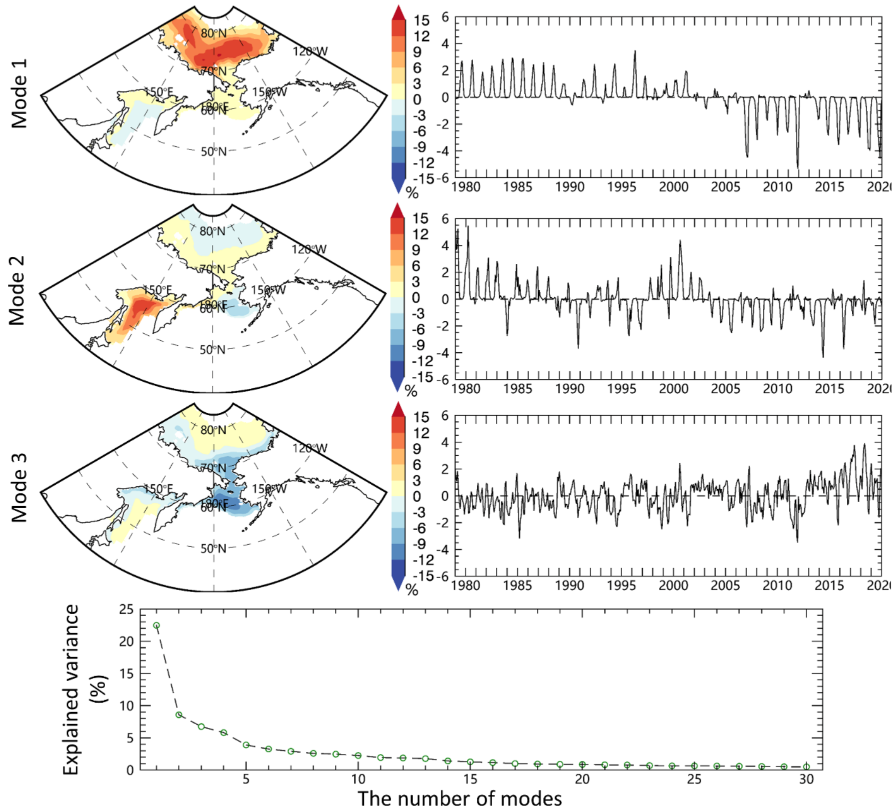

Figure 2. The eigenvectors and PCs of the leading three EOF modes of SIC in the Arctic Pacific sector for the period 1979-2020. The bottom panel shows the explained variance as a function of the number of leading modes of SIC.

3.2 Construct an optimal model for each season

A practical issue in building a Markov model in MEOF spaces is which combination of variables and number of leading modes to retain in the model. Using too few modes may miss some predictable signals, and too many may result in overfitting and contaminate the model with incoherent small-scale features. To determine optimal predictor variables and reasonable mode truncations, we calculate the prediction skill from a series of cross-validated model experiments, which used different numbers of modes and different variables. Table 1 shows the detailed variable-combinations. Models V2-V7 and V9 are weighted towards surface thermodynamic processes, whereas V8 and V10 represent integration of thermodynamic and dynamic processes.

Table 1. Variable combinations in cross-validated experiments. V1 represents the No. 1 variable-combination. √ represents the variable included in the corresponding combination.

	V1	V2	V3	V4	V5	V6	V7	V8	V9	V10
SIC	√	√	√	√	√	√	√	√	√	√
SST		√	√	√	√	√	√	√	√	√
SAT			√			√	√	√	√	√
Surface net turbulent heat flux				√		√			√	√
Surface net radiative flux					√		√		√	√
850hPa GPH, U, V								√		√

The cross-validation scheme is carried out for the time series to produce predictions at 1- to 12-month lead. The PGS and mean RMSE for each lead time in each season are calculated. To avoid missing predictable signals, we initially allow large amounts of modes (up to 52) in the model and then narrow the range of mode numbers to determine the best model configuration for each season. Figure S2 presents the PGS for each lead time for winter target months. It shows that the model prediction skill in winter steeply decreases after 32 modes in most lead months. Similarly, RMSE increases rapidly after 32 modes (Figure S3). This indicates that including modes beyond mode 32 in winter, mainly representative of unpredictable small-scale features, leads to the rapid decrease of predictive skill.

To select a model configuration that fits all lead times, we average the 12 panels in Figures S2 and S3, respectively, and display them in the first column of Figure S4. Similarly, predictive skills for other seasons are also examined. We further shrink the modes' range to display the predictive skill according to Figure S4 so that we can determine the optimal model more accurately (Figure 3). Altogether, the model skills are better in summer and autumn than in winter and spring, and more modes are needed in the cold season to capture the predictable signal of SIC. This indicates that sea ice in the cold season has requires more modes to capture its variability, likely due

https://doi.org/10.5194/tc-2021-284
Preprint. Discussion started: 21 September 2021

to the weaker trends in these months. Models with high correlation also have smaller RMSE but the RMSE differences between models are relatively small. Based on the PGS and RMSE, we primarily chose three superior model configurations marked by black boxes in Figure 3 for winter, summer, and autumn respectively, and chose five superior models in spring since high predictive skills are scattered.

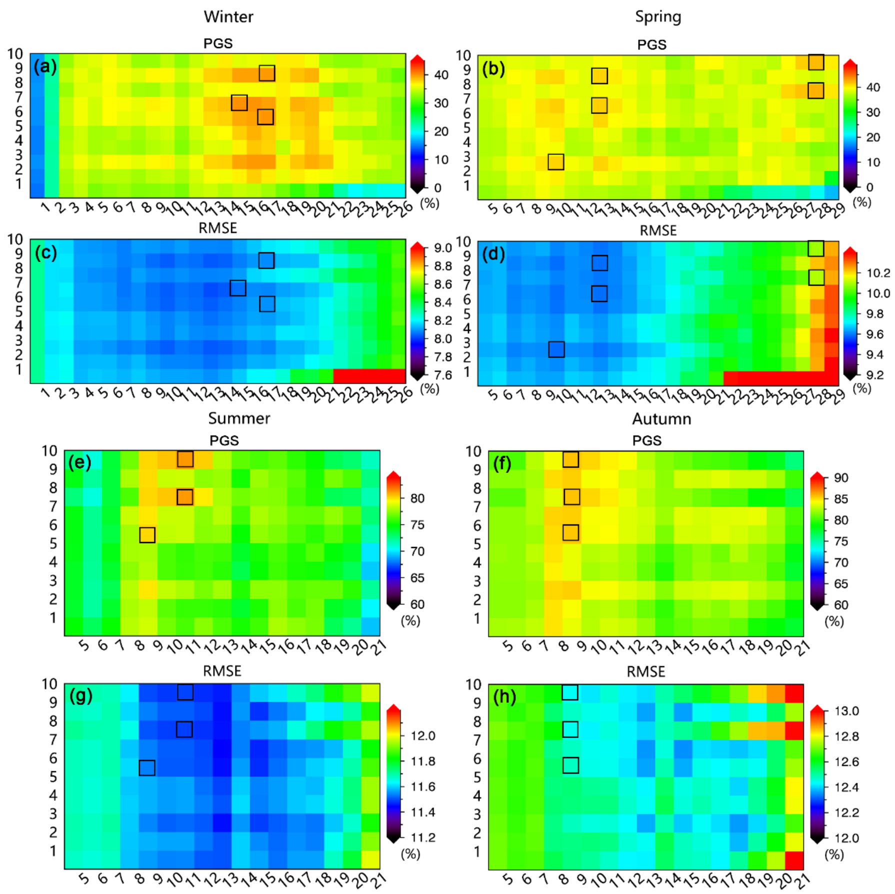

Figure 3. Mean PGS and mean RMSE between the observations and predictions in four seasons. (a) Mean PGS is obtained by averaging all lead months for winter predictions. The x-axis represents the number of MEOF modes, and the y-axis represents the combination of the variables corresponding to Table 1. (b, e, and f) are the same as (a) except for spring, summer, and autumn respectively. (c, d, g, and h) are the same as (a, b, e, and f) except for RMSE.

https://doi.org/10.5194/tc-2021-284
Preprint. Discussion started: 21 September 2021

To determine which model configuration produces the best prediction in each season, we spatially average the SIC prediction skill from these superior models with 1- to 12-month leads (Figures 4 and 5). Figure 4 shows the cross-validation skill measured by PGS. In general, the predictive skill in summer and autumn is higher (by roughly 35%) than that in winter and spring, although the RMSEs are also relatively large in the warm season (Figure 5). These models also exhibit a local minimum of PGS in each season at a 10-month lead for winter, at a 3-month lead for spring, at a 4- and 6-month lead for summer, and at a 7-month lead for autumn. In other words, the seasonal models show a common feature of low prediction skill for forecasts initialized in the month of March, but show higher skill at lead times beyond this, suggesting that certain sources of predictability present in March are absent in these models.

As a model construction principle, we choose the minimum number of variables and modes to achieve the same level of skill, avoiding possible overfitting. Based on the PGS and RMSE, we chose V7M15 as the best model in winter since it shows the lowest RMSE. In spring, we ruled out V8M28 and V10M28 because of the large RMSE and chose V7M13 since it shows a slightly larger correlation among the rest of the models. In the warm season, V8 and V10 show nearly the same skill, indicating that the surface turbulent heat flux and radiative flux do not contribute to the model skill. So we selected the V8M11 in summer and V8M9 in autumn.

In addition to SIC, SST, and SAT, the surface net radiative flux mainly contributes to the model skill in the cold season, reflecting that the surface longwave radiation plays a significant role in the polar climate system in the cold season when shortwave radiation is at its annual minimum. Previous studies suggested that cloud cover is capable of controlling sea ice growth processes through its influences on the surface energy budget via transmitting longwave radiation (Huang et al., 2015; Kapsch et al., 2013; Lee et al., 2017; Liu and Key, 2014; Luo et al., 2017; Wang et al., 2019). On the other hand, Schweiger et al. (2008) argued that negative cloud anomalies combined with increased surface solar radiation in summer had no

https://doi.org/10.5194/tc-2021-284
Preprint. Discussion started: 21 September 2021

substantial contribution to the minimum SIE record in 2007. Nussbaumer and Pinker (2012) conclude that the accumulation of surface downwelling shortwave radiation did not correspond well to negative SIC anomalies in summer. Our model experiments also suggest that the surface net radiative flux does not contribute to the prediction skill in warm season. Instead, 850 hPa GPH and wind, not only affect the heat and moisture transport by atmospheric circulation anomaly but also drive sea-ice drift, mainly contribute to the model skill in warm season. For example, the dipole structure anomaly of the Arctic atmospheric circulation shows strong meridionality and plays a profound role in sea-ice export/import, and heat and moisture transport through the Pacific-Arctic sector (Wu et al., 2005).

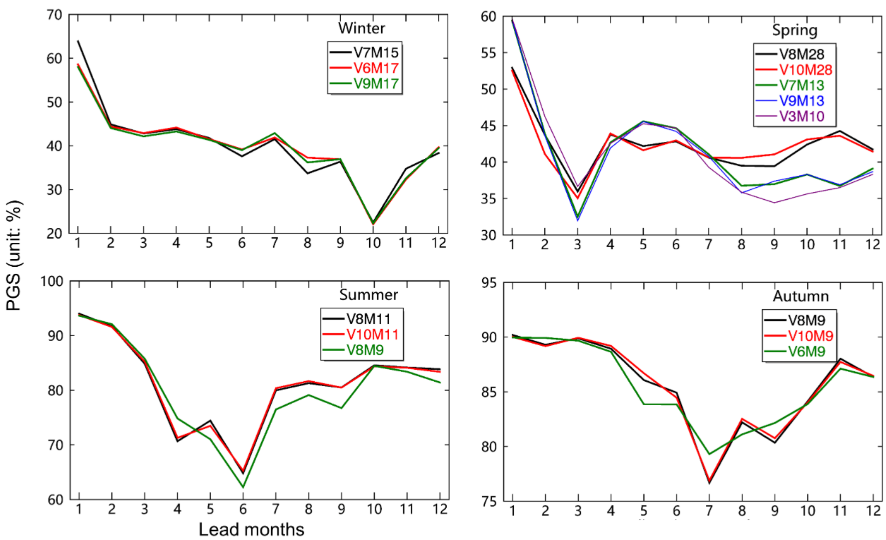

Figure 4. PGS for the preliminary selection of superior models in each season.

https://doi.org/10.5194/tc-2021-284
Preprint. Discussion started: 21 September 2021

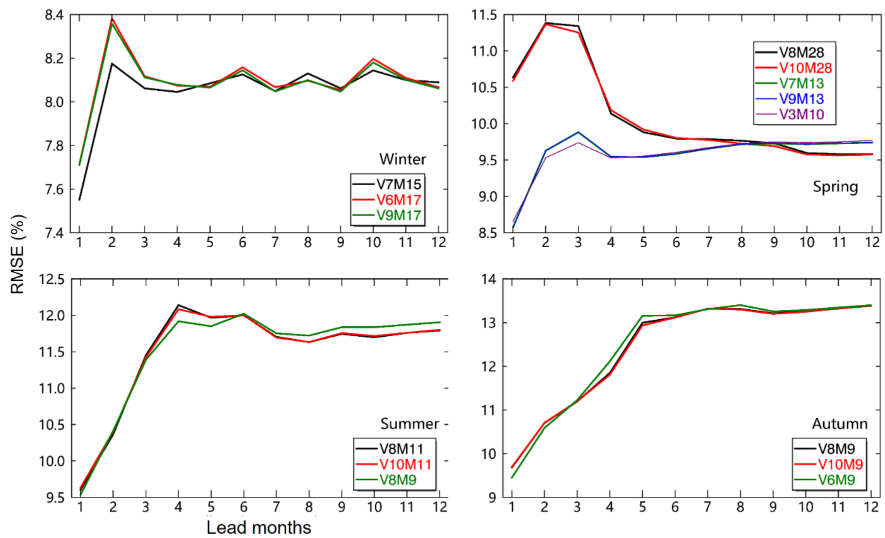

Figure 5. Same as Figure 4 but for RMSE.

3.3 Assessment of model skill

To test the forecast skill of the model, the SIC predictions were evaluated at each grid cell and for all seasons using the ACC and RMSE between predicted and observed anomalies, and the skill is presented at 3, 6, 9, and 12 lead months. In winter (DJF), high forecast skill is concentrated in the Arctic marginal seas and peripheral seas: the northern Bering Strait and northern Sea of Okhotsk (Figure 6). The skill is slightly lower at a 6-month lead in the Sea of Okhotsk and from a 6-month to 9-month lead in the Bering Sea, whereas high skill values (>0.6) are maintained up to a 12-month lead in the Bering Strait. The spring (MAM) prediction skill shows a similar pattern as that in winter but with a 0.1 reduction in the ACC skill. The southern Chukchi Sea and Bering Strait have higher skills than the southern part of the strait. For summer (JJA) predictions, the prediction skill is concentrated in the Arctic basin since sea ice nearly totally melts in the Arctic peripheral seas. The 3-month lead prediction has the highest skill (>0.6) in most of the Arctic basin, while the lowest prediction skill (<0.4) is found at a 6-month lead. This skill dip indicates that using winter SIC to forecast summer sea ice is unsatisfactory. However, the 9-month and 12-month lead predictions again show high skill (>0.6) in most of the Arctic Basin.

https://doi.org/10.5194/tc-2021-284
Preprint. Discussion started: 21 September 2021

The autumn (SON) prediction skill shows a similar pattern but with higher correlations than that in summer. For targeted autumn predictions, the significantly increased skill at 6-month lead relative to other seasons could be related to the sea ice anomaly reemergence from spring to autumn due to the oceanic memory (Blanchard-Wrigglesworth et al., 2011). Still, the autumn prediction skill at a 6-month lead is lower than that at other lead months, indicating that the impact of the spring predictability barrier on prediction was not offset by the SST anomaly reemergence. In general, the model has higher prediction skills for warm seasons, especially for autumn, than that for cold seasons, while the lowest skill is in spring.

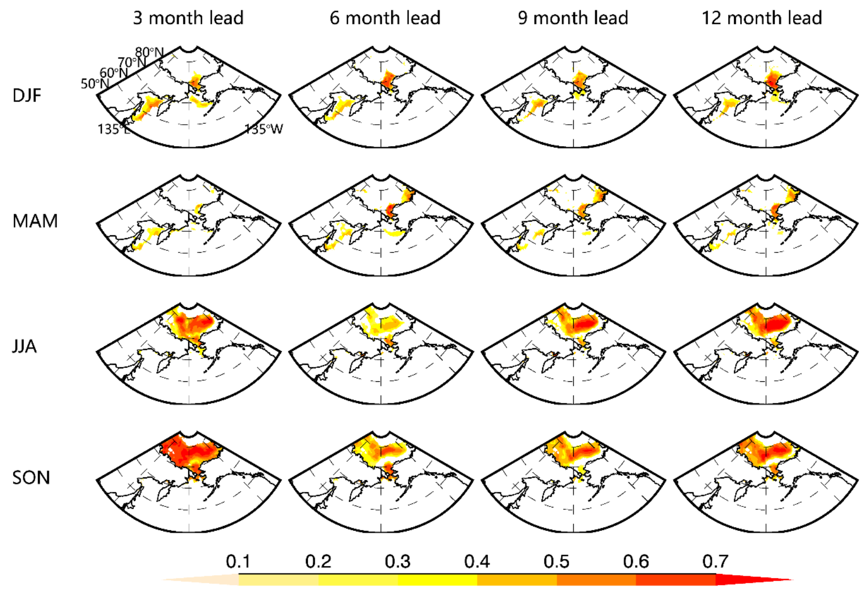

Figure 6. Cross-validated model skills measured by ACC between SIC predictions and observation anomalies as a function of seasons and lead months. Only the correlations that are significantly above the 95% confidence level based on a Student's t test are included in the panels.

RMSEs are consistent with correlations: high correlations correspond to low RMSEs, and vice versa, although minor inconsistencies occur in some seasons and regions (Figure 7). The RMSE is large around the Arctic basin for the warm season and in the peripheral sea for the cold season where SIC has large variability. In the

https://doi.org/10.5194/tc-2021-284
Preprint. Discussion started: 21 September 2021

cold season, the RMSE is larger in the Bering Sea than that in the Sea of Okhotsk. The magnitudes of RMSE remain at roughly the same level from 3- to 12-month lead and all seasons in most locations. The marginal seas have larger RMSEs than the central Arctic basin in both summer and autumn, while the error magnitudes in autumn are slightly larger than those in summer but smaller than the SIC standard deviation across the Pacific sector (Figure 1).

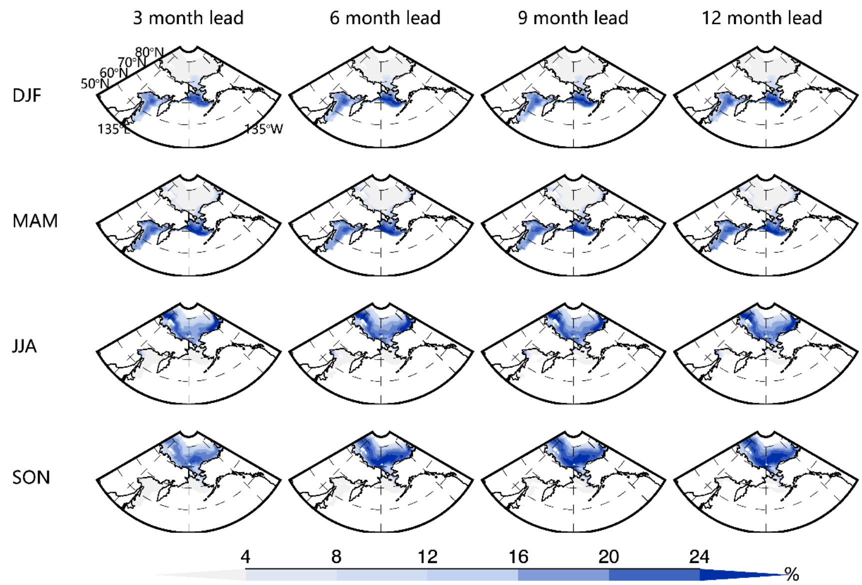

Figure 7. Same as Figure 6 except for RMSEs. The color bar is in a unit of %.

Also, the model performance is further evaluated against anomaly persistence and climatology. Averaged over the grid points in the model domain and over all seasons for the period of 1980-2020, the regional Markov model's mean correlation is manifestly higher, and the mean RMSE of the regional Markov model is still quite skillful compared with the climatology and anomaly persistence for all the lead months whether the sea ice trend is removed or not, especially from 2-month lead to 10-month lead (Figure 8). In addition, RMSE is not sensitive to the lead months, showing the superiority of the regional model. This indicates that there are crucial sources of predictability beyond SIC anomaly persistence that the regional Markov model is able to capture.

https://doi.org/10.5194/tc-2021-284
Preprint. Discussion started: 21 September 2021

The Cryosphere
Discussions
Open Access

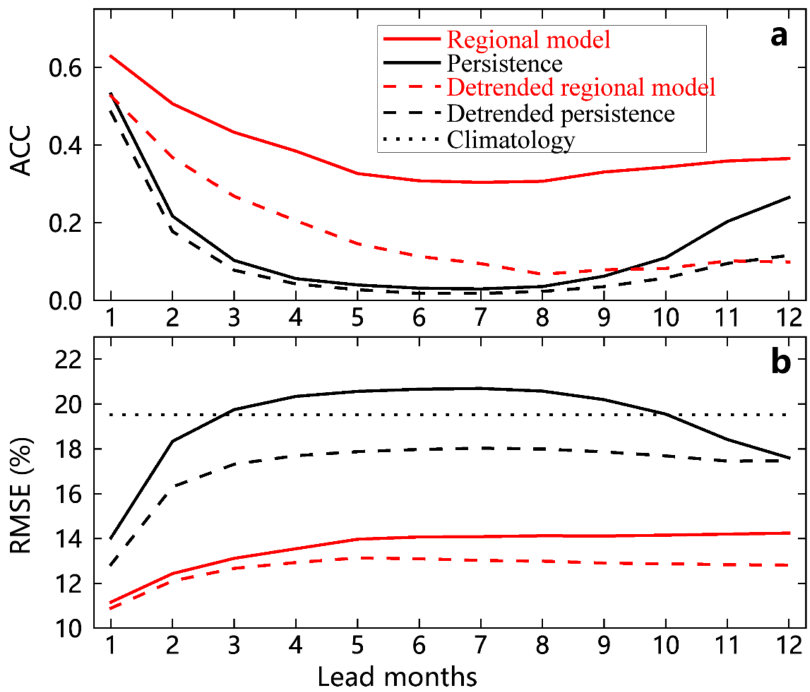

Figure 8. The prediction skill of the regional Markov model compared against that of anomaly persistence and climatology as a function of the number of month lead times.

To assess the regional model skill improvements from the pan-Arctic model presented by Yuan et al. (2016), we calculated the PGS and ACC as a function of lead months (Figure 9). Note that the PGS is calculated in the entire area for the Bering Sea and the Sea of Okhotsk, and the ACC is calculated only in typical regions with large standard deviations marked in Figure 1. The regional model substantially enhances the PGS skill from the pan-Arctic model for the 2- to 12-month lead predictions in the Bering Sea and the 1- to 7-month lead predictions in the Sea of Okhotsk. The PGS improvement is 75% in the Bering Sea and 16% in the Sea of Okhotsk. Similarly, the ACC is also increased by 21% in the Bering Sea and 8% in the Sea of Okhotsk. The prediction skill of the regional Markov model in the Arctic basin also remains at the same high level as that of the Pan-Arctic model (not shown),

https://doi.org/10.5194/tc-2021-284
Preprint. Discussion started: 21 September 2021

so significant skill improvements occur in the peripheral sea of the Pacific sector, demonstrating the superiority of the regional model.

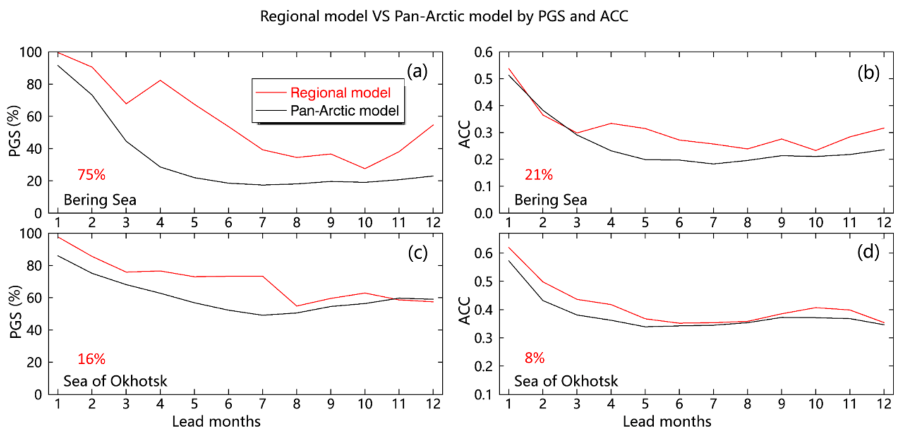

Figure 9. Cross-validated model skills of the regional Markov model vs. the Pan-Arctic Markov model. (a, c) The skills are measured by the PGS between predictions and observations from 1980 to 2020 as a function of lead months in the Bering Sea and the Sea of Okhotsk. (b, d) are the same as (a, c) except for the ACC. The red numbers in the left bottom of each panel represent the regional model skill improvements from the pan-Arctic model.

3.4 Contribution of linear trends to SIE prediction skill

Sigmond et al. (2013) show that the linear trend in Arctic SIE dramatically contributes to its forecast skill in the Canadian Seasonal to Interannual Prediction System. Lindsay et al. (2008) show that their dynamic model prediction skill is much lower when the trend is not included. They suggested that the trend accounts for 76% of the variance of the pan-Arctic ice extent in September. The trend also contributes to the pan-Arctic prediction in the linear Markov model (Yuan et al., 2016). In the Arctic, SIE has declined at -0.35 million square kilometers per decade during 1979-2020, which is significant at the 95% confidence level. The large SIC trend is mainly in the Barents Sea and the Kara Sea, followed by the Chukchi Sea, while the mean SIC trend in the Bering Sea and the Sea of Okhotsk is relatively weak (Figure 1). To evaluate the contribution of long-term trends to the regional Markov model skill, we

https://doi.org/10.5194/tc-2021-284
Preprint. Discussion started: 21 September 2021

examine the time series of SIE in all calendar and lead months calculated by summing the Pacific areas that have at least 15% SIC from observations and predictions. Then, the model skill is compared between the original SIE predictions and detrended SIE predictions.

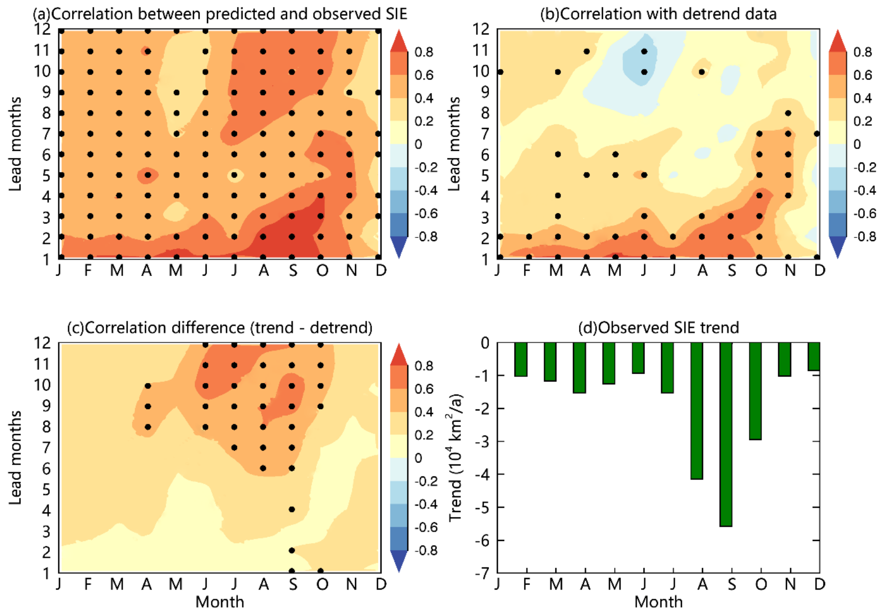

Figure 10. (a) The SIE forecast skill of the regional Markov model as a function of the calendar month and lead months. (b) The SIE forecast skill when monthly trends are removed from the predictions and observations. The black dots in (a) and (b) represent the correlations that are significantly above the 95% confidence level. (c) Difference between (a) and (b). The black dots in (c) indicate that the correlation differences are significant above the 95% confidence level. (d) Observed trends in SIE as a function of the calendar month. All monthly SIE trends are significantly above the 95% confidence level.

Figure 10 shows the model skill of the SIE forecast in the Arctic Pacific sector and the contribution of linear trends to the skill. The model has good skill predicting SIE from January to November at a 1- to 2-month lead (Figure 10a). The skill is particularly high for the predictions in summer and autumn. It is higher than 0.6 from July through October even at lead months 9-12. The model skill is relatively low in May and December especially at 8-11 lead months. This pattern is consistent with the seasonal variation of the model skill for SIC prediction presented in Figure 6.

After monthly trends are removed from both predictions and observations, the model skill is significantly reduced for all seasons, especially for the warm season at 6-12 months lead (Figure 10b, c). This is consistent with the seasonality of the observed trend (Figure 10d), which also peaks in late summer and early fall. Averaging the differences in Figure 10c over all lead times and predicted months, the trend removal results in a mean reduction of 0.3 from the SIE forecast skill; a 55% reduction of the mean ACC. However, the model retains high prediction skill (0.63) from January to October at 1-2 lead months, representing a 16% reduction by trend removal in these leads (Figure 10b), which shows the model's capability of capturing sea ice internal variability. In addition, the trend is relatively large in the Chukchi Sea and weak outside of the Arctic Ocean. The model only reduces 11% of the mean ACC from January to October at 1-2 lead months after the trend removal for the area outside of the Arctic Ocean.

3.5 Comparison with the GFDL model

Yuan et al. (2016) showed that the pan-Arctic Markov model consistently outperforms the NOAA/NCEP Climate Forecast System (CFSv2) and the Canadian seasonal and interannual prediction system for sea ice seasonal predictions. Here the regional Markov model is compared with the Geophysical Fluid Dynamics Laboratory Forecast-oriented Low Ocean Resolution (GFDL-FLOR) seasonal prediction system (Bushuk et al., 2017). The hindcast model skill measured by the ACC for detrended SIE are high from both the regional Markov model and GFDL seasonal prediction system during January to June at a 1- to 3-month lead in the Pacific sector (Figure 11). The regional Markov model skill is statistically significant at lead times ranging from 1 to 5 months for target months of January-June in both the

https://doi.org/10.5194/tc-2021-284
Preprint. Discussion started: 21 September 2021

Bering Sea and the Sea of Okhotsk. Below we highlight some key differences between these two models in the Bering Sea and the Sea of Okhotsk.

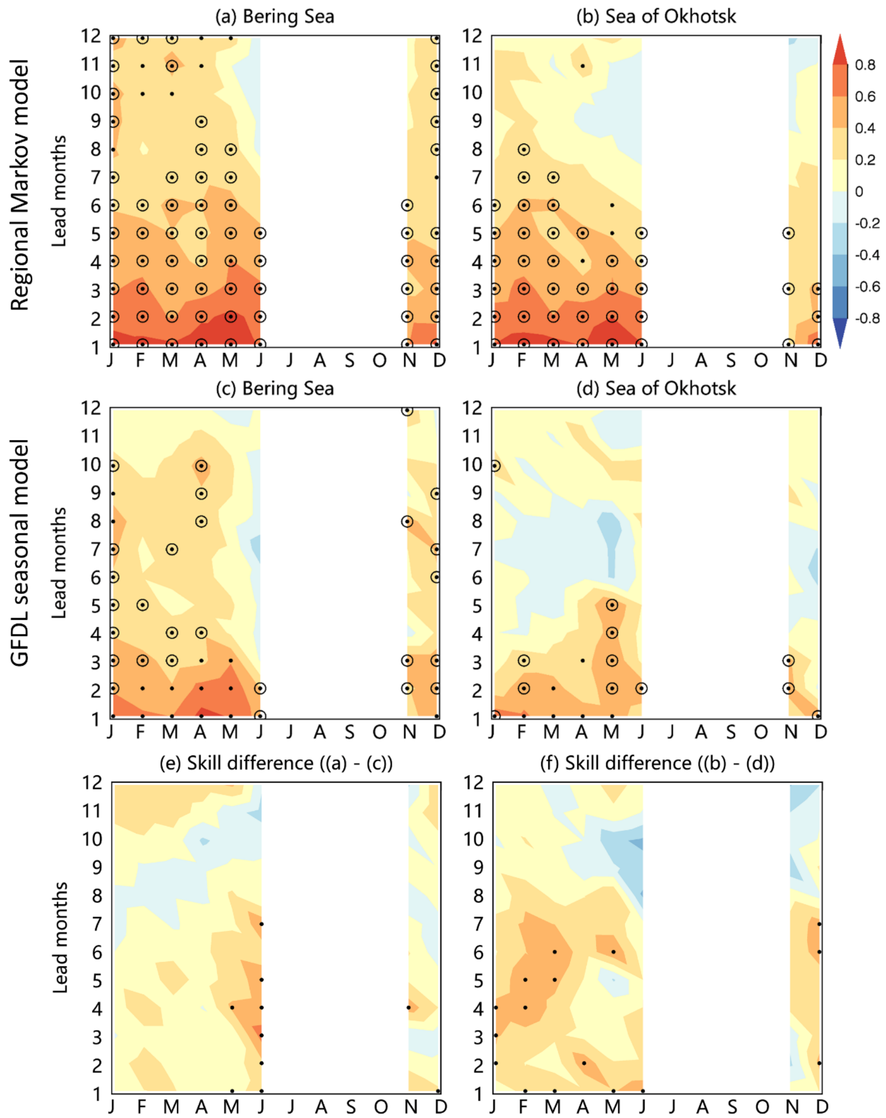

Figure 11. (a, b) Hindcast model skill (ACC) for detrended regional SIE from 1982 to 2020 for the regional Markov model. (c, d) Same as (a, b) except for the GFDL seasonal prediction system. (e, f) is the skill difference between these two models. The black dots in (a-d) represent ACCs that are significantly above the 95%

https://doi.org/10.5194/tc-2021-284
Preprint. Discussion started: 21 September 2021

confidence level, and the circles in (a-d) indicate months in which the model's skill exceeds that of a persistence forecast. The black dots in (e-f) represent ACC differences that are significant above the 95% confidence level.

Notably, the skill from the regional Markov model is higher than that from the GFDL seasonal prediction system in June at 1- to 7-month leads in the Bering Sea and during December to March at 1- to 7-month leads in the Sea of Okhotsk. In the other words, the regional Markov model performs better in June prediction using the observations in the previous winter and spring in the Bering Sea. The model also performs better in winter to early spring prediction using the observations in previous summer and fall in the Sea of Okhotsk. Nevertheless, the regional Markov model slightly underperforms the GFDL seasonal prediction system for cold season predictions using the previous summer observations in the Bering Sea, and for early summer predictions using previous early fall observations in the Sea of Okhotsk. It indicates that the weakness of the regional Markov model is mainly reflected in the SIE prediction using the previous late summer and early fall observations compared with the GFDL seasonal prediction system, which is likely because the surface climate anomaly in late summer/early fall loses its identity in fall and does not contribute to winter sea ice variability. Overall, the regional Markov model delivers skillful predictions in seasonal ice zones of the Pacific sector up to 6 month lead times, an improvement from the 3 month leads displayed in the GFDL seasonal prediction system.

4 Conclusions

Here, we developed a regional Markov model to predict SIC in the Arctic Pacific sector at the seasonal time scale. The model was constructed in the MEOF space so that the model can capture the covariability of the North Pacific climate system defined by 7 variables (SIC, SST, SAT, surface net radiative flux, surface net turbulent heat flux, and geopotential height and winds at 850 hPa). Based on cross-validation experiments, we selected model variables and mode truncations that provided the best results in each season. These model configurations were V7M15 for winter, V7M13 for spring, V8M11 for summer, and V8M9 for autumn. The V7 models utilize SIC, SST, SAT, and surface net radiative flux as predictor variables, whereas the V8 models use SIC, SST, SAT, winds and geopotential height.

The SIC prediction skill was evaluated at each grid and for all seasons using ACC. The winter skill is 0.4 in the Sea of Okhotsk and 0.5 in the Bering Strait at up to 12-month leads. The spring prediction shows a similar pattern but with a 0.1 reduction in the ACC skill. The model skill in summer and autumn is 0.6 in the Arctic basin. Compared with the pan-Arctic seasonal prediction model (Yuan et al., 2016), the regional Markov model distinctly improves the SIC prediction skill in the Arctic Pacific sector. The regional model significantly enhances the correlation skill from the pan-Arctic model for 2- to 12-month lead predictions in the Bering Sea and 1- to 7-month lead predictions in the Sea of Okhotsk. The improvement measured by the PGS is 75% in the Bering Sea and 16% in the Sea of Okhotsk. The ACC is also increased by 21% in the Bering Sea and 8% in the Sea of Okhotsk. In addition, similar to the pan-Arctic Markov model, the regional model is not sensitive to the number of MEOF modes retained, which indicates that the performance of this Markov model is robust. Additionally, the regional Markov model's skill is superior to the skill derived from anomaly persistence, revealing the model’s ability to capture more predictable SIC internal variability than anomaly persistence.

The model retains prediction skill regardless of whether the sea ice trend is removed or not, however, the detrended skill is notably lower, consistent with earlier sea ice prediction studies. When sea ice time series includes the trend, the model has good skill at predicting SIE from January to November. The skill is particularly high for the predictions of summer and autumn sea ice at longer lead times, especially in July to October when the skill is high (>0.6) even at 9-12 lead months. The model skill is relatively low in May and December especially at 8-11 lead months. Trend removal from both predictions and observations results in a 55% reduction of the mean ACC for the entire Arctic Pacific sector. However, the model only reduces 11%

of the mean ACC from January to October at 1-2 lead months after the trend removal for the North Pacific sector, including the Bering Sea and the Sea of Okhotsk. This detrended analysis shows the model's capability of capturing sea ice internal variability. Furthermore, the regional Markov model improves the detrended SIE prediction skill in the Pacific sector to 6 month lead times from the 3 month lead skill displayed in the GFDL-FLOR seasonal prediction system.

The following reasons contribute to the improvements. First, the dominant climate variability in the northern mid-high latitudes mostly occurs in the Atlantic sector of the Arctic and subarctic, which dictates the leading MEOF mode in the pan-Arctic model. The unique characteristics of atmosphere-ocean-sea ice coupled relationships in the Pacific sector may not be included in the leading MEOF decompositions of the pan-Arctic climate system and thus are not correctly represented in the model. The regional model focuses on the Pacific-Arctic coupled atmosphere-ocean-sea ice system and captures the dominant regional climate variability. Second, the Pacific sector of the Arctic needs a different set of variables to maximize the model's predictability. We added surface net radiative flux, which partially controls the sea-ice growth processes through its influences on the surface energy budget. We also include 850 hPa GPH and winds to represent dynamic atmospheric processes. Finally, we constructed a superior model for each season, isolating the seasonally dominant processes separately.

The sensitivity experiments revealed that surface longwave radiation plays a significant role in the Pacific Arctic climate system variability in cold seasons when shortwave radiation is at its annual minimum. The 850 hPa GPH and winds mainly contribute to the model skill in warm seasons, reflecting that the influence of atmospheric circulation on sea ice is more easily captured by MEOF in warm seasons than in the cold season. It was also found that more modes were needed in the cold season to capture the predictable signal of SIC. This suggests that sea ice in cold seasons has more variability patterns compared with that in warm seasons, which may bring more errors in prediction. SIC trends are also strongest in the warm season

https://doi.org/10.5194/tc-2021-284
Preprint. Discussion started: 21 September 2021

months, which may contribute to the smaller number of modes required. In addition to the climate system in the Arctic Basin, the coupled atmosphere-ocean-sea ice variability in the North Pacific plays a more important role in the cold season and needs more modes to capture the covariability signals.

However, weaknesses of the model remain. The summer initialization months have little sea ice coverage, and SST does not provide enough memory for winter predictions in the Bering Sea and the Sea of Okhotsk due to shallow summer mixed layers. Thus, other sources of memory are required to provide sea ice prediction skill in cold seasons. By the mechanism for mid-latitude SST reemergence, subsurface ocean temperature anomalies in summer would potentially impact sea ice growth rates the following cold season (Bushuk et al., 2017; Bushuk et al., 2020). These deficiencies provide us with opportunities for improvements in future work.

Data availability. The sea ice concentration data were obtained from the National Snow and Ice Data Center (NSIDC, https://nsidc.org/data/NSIDC-0079, last access: 1 July 2021, Comiso, 2017). The sea surface temperature, surface air temperature, surface net radiative flux, surface net turbulent heat flux, 850hPa geopotential height, and 850hPa wind vector from the ERA5 can be obtained from the ECMWF (https://cds.climate.copernicus.eu/cdsapp#!/search?type=dataset, last access: 1 July 2021, Hersbach et al., 2020).

Supplement. The supplement related to this article is available online at: **xxxx**.

Author contributions. YW, XY and HB conceived the idea for the protocol and experiment design. MB and HH provided primary support and guidance on the research. YW, YL and CL performed data processing. All authors drafted the manuscript, and contributed to the manuscript revision.

Competing interests. The authors declare that they have no conflict of interest.

https://doi.org/10.5194/tc-2021-284
Preprint. Discussion started: 21 September 2021

Acknowledgements. This work is supported by the Lamont endowment, the National Natural Science Foundation of China (42106223), and the China Postdoctoral Science Foundation (2020TQ0322). We thank the NSIDC for providing the sea ice concentration data on their website (https://nsidc.org/data/NSIDC-0079). The sea surface temperature, surface air temperature, surface net radiative flux, surface net turbulent heat flux, 850hPa geopotential height, and 850hPa wind vector from the ERA5 can be obtained from the ECMWF (https://cds.climate.copernicus.eu/cdsapp#!/search?type=dataset).

Financial support. This work is supported by the Lamont endowment, the National Natural Science Foundation of China (42106223), and the China Postdoctoral Science Foundation (2020TQ0322).

Lamont contribution number xxxx.

References

Barnston, A. G. and Ropelewski, C. F.: Prediction of ENSO Episodes Using Canonical Correlation Analysis, J. Clim., 5, 1316-1345, https://doi.org/10.1175/1520-0442(1992)005<1316:poeeuc>2.0.co;2, 1992.

Blanchard-Wrigglesworth, E., Armour, K. C., Bitz, C. M., and Deweaver, E.: Persistence and Inherent Predictability of Arctic Sea Ice in a GCM Ensemble and Observations, J. Clim., 24, 231-250, https://doi.org/10.1175/2010JCLI3775.1, 2011.

Blanchard-Wrigglesworth, E., Cullather, R., Wang, W., Zhang, J., and Bitz, C.: Model forecast skill and sensitivity to initial conditions in the seasonal Sea Ice Outlook, Geophys. Res. Lett., 42, 8042-8048, https://doi.org/10.1002/2015GL065860, 2015.

Bushuk, M., Msadek, R., Winton, M., Vecchi, G. A., Gudgel, R., Rosati, A., and Yang, X.: Skillful regional prediction of Arctic sea ice on seasonal timescales, Geophys. Res. Lett., 44, 4953-4964, https://doi.org/10.1002/2017GL073155, 2017.

Bushuk, M., Winton, M., Bonan, D. B., Blanchard-Wrigglesworth, E., and Delworth, T. L.: A Mechanism for the Arctic Sea Ice Spring Predictability Barrier, Geophys. Res. Lett., 47, https://doi.org/10.1029/2020gl088335, 2020.

Cañizares, R., Kaplan, A., Cane, M. A., Chen, D., and Zebiak, S. E.: Use of data assimilation via linear low-order models for the initialization of El Niño-Southern Oscillation predictions, Journal of Geophysical Research: Oceans, 106, 30947-30959, https://doi.org/10.1029/2000JC000622, 2001.

https://doi.org/10.5194/tc-2021-284
Preprint. Discussion started: 21 September 2021

Chen, D. and Yuan, X.: A Markov model for seasonal forecast of Antarctic sea ice, J. Clim., 17, 3156-3168, https://doi.org/10.1175/1520-0442(2004)017<3156:AMMFSF>2.0.CO;2, 2004.

Cohen, J., Zhang, X., Francis, J., Jung, T., Kwok, R., Overland, J., Ballinger, T., Bhatt, U., Chen, H., and Coumou, D.: Divergent consensuses on Arctic amplification influence on midlatitude severe winter weather, Nature Climate Change, 10, 20-29, https://doi.org/10.1038/s41558-019-0662-y, 2020.

Comiso, J. C.: Bootstrap Sea Ice Concentrations from Nimbus-7 SMMR and DMSP SSM/I-SSMIS, Version 3. NASA National Snow and Ice Data Center Distributed Active Archive Center, Boulder, Colorado USA, 2017.

Day, J. J., Tietsche, S., and Hawkins, E.: Pan-Arctic and Regional Sea Ice Predictability: Initialization Month Dependence, J. Clim., 27, 4371-4390, https://doi.org/10.1175/JCLI-D-13-00614.1, 2014.

Deser, C., Tomas, R., Alexander, M., and Lawrence, D.: The seasonal atmospheric response to projected Arctic sea ice loss in the late twenty-first century, J. Clim., 23, 333-351, https://doi.org/10.1175/2009JCLI3053.1, 2010.

Francis, J. A. and Vavrus, S. J.: Evidence linking Arctic amplification to extreme weather in mid-latitudes, Geophys. Res. Lett., 39, https://doi.org/10.1029/2012GL051000, 2012.

Frankignoul, C., Sennechael, N., and Cauchy, P.: Observed Atmospheric Response to Cold Season Sea Ice Variability in the Arctic, J. Clim., 27, 1243-1254, https://doi.org/10.1175/jcli-d-13-00189.1, 2014.

Guemas, V., Blanchard-Wrigglesworth, E., Chevallier, M., Day, J. J., Déqué, M., Doblas-Reyes, F. J., Fučkar, N. S., Germe, A., Hawkins, E., and Keeley, S.: A review on Arctic sea-ice predictability and prediction on seasonal to decadal time-scales, QJRMS, 142, 546-561, https://doi.org/10.1002/qj.2401, 2016.

Hamilton, L. C. and Stroeve, J.: 400 predictions: The search sea ice outlook 2008–2015, Polar Geogr, 39, 274-287, https://doi.org/10.1080/1088937X.2016.1234518, 2016.

Hersbach, H., Bell, B., Berrisford, P., Hirahara, S., Horányi, A., Muñoz-Sabater, J., Nicolas, J., Peubey, C., Radu, R., and Schepers, D.: The ERA5 global reanalysis, QJRMS, 146, 1999-2049, https://doi.org/10.1002/qj.3803, 2020.

Huang, Y., Dong, X., Xi, B., Dolinar, E. K., and Stanfield, R. E.: Quantifying the Uncertainties of Reanalyzed Arctic Cloud and Radiation Properties using Satellite-surface Observations, ClDy, 30, 8007-8029, https://doi.org/10.1175/JCLI-D-16-0722.1, 2015.

Kapsch, M. L., Graversen, R. G., and Tjernström, M.: Springtime atmospheric energy transport and the control of Arctic summer sea-ice extent, Nature Climate Change, 3, 744-748, https://doi.org/10.1038/nclimate1884, 2013.

Kim, K.-Y., Hamlington, B. D., Na, H., and Kim, J.: Mechanism of seasonal Arctic sea ice evolution and Arctic amplification, The Cryosphere, 10, 2191-2202, https://doi.org/10.5194/tc-10-2191-2016, 2016.

Koenigk, T., Caian, M., Nikulin, G., and Schimanke, S.: Regional Arctic sea ice variations as predictor for winter climate conditions, ClDy, 46, 317-337, https://doi.org/10.1007/s00382-015-2586-1, 2016.

Lee, S., Gong, T., Feldstein, S. B., Screen, J. A., and Simmonds, I.: Revisiting the Cause of the 1989–2009 Arctic Surface Warming Using the Surface Energy Budget: Downward Infrared

https://doi.org/10.5194/tc-2021-284
Preprint. Discussion started: 21 September 2021

Radiation Dominates the Surface Fluxes, Geophys. Res. Lett., 44, 10654-10661, https://doi.org/10.1002/2017GL075375, 2017.

Lindsay, R., Zhang, J., Schweiger, A., and Steele, M.: Seasonal predictions of ice extent in the Arctic Ocean, Journal of Geophysical Research: Oceans, 113, https://doi.org/10.1029/2007JC004259, 2008.

Liu, Y. and Key, J. R.: Less winter cloud aids summer 2013 Arctic sea ice return from 2012 minimum, Environmental Research Letters, 9, 044002, https://doi.org/10.1088/1748-9326/9/4/044002, 2014.

Luo, B., Luo, D., Wu, L., Zhong, L., and Simmonds, I.: Atmospheric circulation patterns which promote winter Arctic sea ice decline, Environmental Research Letters, 12, 1-13, https://doi.org/10.1088/1748-9326/aa69d0, 2017.

Meleshko, V., Kattsov, V., Mirvis, V., Baidin, A., Pavlova, T., and Govorkova, V.: Is there a link between Arctic sea ice loss and increasing frequency of extremely cold winters in Eurasia and North America? Synthesis of current research, Russian Meteorology and Hydrology, 43, 743-755, https://doi.org/10.3103/S1068373918110055, 2018.

Notz, D. and Marotzke, J.: Observations reveal external driver for Arctic sea-ice retreat, Geophys. Res. Lett., 39, https://doi.org/10.1029/2012GL051094, 2012.

Nussbaumer, E. A. and Pinker, R. T.: The role of shortwave radiation in the 2007 Arctic sea ice anomaly, Geophys. Res. Lett., 39, L15808, https://doi.org/10.1029/2012GL052415, 2012.

Peterson, A. K., Fer, I., McPhee, M. G., and Randelhoff, A.: Turbulent heat and momentum fluxes in the upper ocean under Arctic sea ice, Journal of Geophysical Research: Oceans, 122, 1439-1456, https://doi.org/10.1002/2016JC012283, 2017.

Peterson, K. A., Arribas, A., Hewitt, H., Keen, A., Lea, D., and McLaren, A.: Assessing the forecast skill of Arctic sea ice extent in the GloSea4 seasonal prediction system, ClDy, 44, 147-162, https://doi.org/10.1007/s00382-014-2190-9, 2015.

Petty, A., Schröder, D., Stroeve, J., Markus, T., Miller, J., Kurtz, N., Feltham, D., and Flocco, D.: Skillful spring forecasts of September Arctic sea ice extent using passive microwave sea ice observations, Earth's Future, 5, 254-263, https://doi.org/10.1002/2016EF000495, 2017.

Porter, D. F., Cassano, J. J., and Serreze, M. C.: Analysis of the Arctic atmospheric energy budget in WRF: A comparison with reanalyses and satellite observations, Journal of Geophysical Research Atmospheres, 116, https://doi.org/10.1029/2011JD016622, 2011.

Sévellec, F., Fedorov, A. V., and Liu, W.: Arctic sea-ice decline weakens the Atlantic meridional overturning circulation, Nature Climate Change, 7, 604-610, https://doi.org/10.1038/NCLIMATE3353, 2017.

Schweiger, A. J., Lindsay, R. W., Vavrus, S., and Francis, J. A.: Relationships between Arctic sea ice and clouds during autumn, J. Clim., 21, 4799-4810, https://doi.org/10.1175/2008JCLI2156.1, 2008.

Screen, J. A. and Francis, J. A.: Contribution of sea-ice loss to Arctic amplification is regulated by Pacific Ocean decadal variability, Nature Climate Change, 6, 856-860, https://doi.org/10.1038/NCLIMATE3011, 2016.

Screen, J. A., Simmonds, I., Deser, C., and Tomas, R.: The atmospheric response to three decades of observed Arctic sea ice loss, J. Clim., 26, 1230-1248, https://doi.org/10.1175/JCLI-D-12-00063.1, 2013.

https://doi.org/10.5194/tc-2021-284
Preprint. Discussion started: 21 September 2021

Sigmond, M., Fyfe, J. C., Flato, G. M., Kharin, V. V., and Merryfield, W. J.: Seasonal forecast skill of Arctic sea ice area in a dynamical forecast system, Geophys. Res. Lett., 40, 529-534, https://doi.org/10.1002/grl.50129, 2013.

Smith, D. M., Dunstone, N. J., Scaife, A. A., Fiedler, E. K., Copsey, D., and Hardiman, S. C.: Atmospheric response to Arctic and Antarctic sea ice: The importance of ocean–atmosphere coupling and the background state, J. Clim., 30, 4547-4565, https://doi.org/10.1175/JCLI-D-18-0100.1, 2017.

Smith, L. C. and Stephenson, S. R.: New Trans-Arctic shipping routes navigable by midcentury, Proceedings of the National Academy of Sciences, 110, E1191-E1195, https://doi.org/10.1073/pnas.1214212110, 2013.

Swart, N.: Natural causes of Arctic sea-ice loss. 2017.

Wang, Y., Yuan, X., Bi, H., Liang, Y., Huang, H., Zhang, Z., and Liu, Y.: The Contributions of Winter Cloud Anomalies in 2011 to the Summer Sea-Ice Rebound in 2012 in the Antarctic, Journal of Geophysical Research: Atmospheres, 124, 3435-3447, https://doi.org/10.1029/2018JD029435, 2019.

Wu, B., Wang, J., and Walsh, J. E.: Dipole Anomaly in the Winter Arctic Atmosphere and Its Association with Sea Ice Motion, J. Clim., 19, 210-225, https://doi.org/10.1175/JCLI3619.1, 2005.

Wu, Q., Cheng, L., Chan, D., Yao, Y., Hu, H., and Yao, Y.: Suppressed midlatitude summer atmospheric warming by Arctic sea ice loss during 1979–2012, Geophys. Res. Lett., 43, 2792-2800, https://doi.org/10.1002/2016GL068059, 2016.

Wu, Q., Yan, Y., and Chen, D.: A linear Markov model for East Asian monsoon seasonal forecast, J. Clim., 26, 5183-5195, https://doi.org/10.1175/JCLI-D-12-00408.1, 2013.

Xue, Y., Leetmaa, A., and Ji, M.: ENSO prediction with Markov models: The impact of sea level, J. Clim., 13, 849-871, https://doi.org/10.1175/1520-0442(2000)013, 2000.

Yuan, X., Chen, D., Li, C., Wang, L., and Wang, W.: Arctic sea ice seasonal prediction by a linear Markov model, J. Clim., 29, 8151-8173, https://doi.org/10.1175/JCLI-D-15-0858.1, 2016.